Ceramics International 43 (2017) 2511–2516

Contents lists available at ScienceDirect

Ceramics International

journal homepage: www.elsevier.com/locate/ceramint

The effect of sputtering atmosphere parameters on dielectric properties of the ferromagnetic alloy – ferroelectric ceramics nanocomposite $(FeCoZr)_x(PbZrTiO_3)_{(100-x)}$

Oleksandr Boiko[a], Tomasz N. Koltunowicz[a,*], Pawel Zukowski[a], Alexander K. Fedotov[b], Andrey V. Larkin[b]

[a] Department of Electrical Devices and High Voltage Technology, Lublin University of Technology, 20-618 Lublin, Poland
[b] Department of Energy Physics, Belarusian State University, 220030 Minsk, Belarus

ARTICLE INFO

Keywords:
Nanocomposites
Ferroelectric
Ceramics
Ion beam sputtering
AC conductivity
Relaxation time
Activation energy

ABSTRACT

Two samples of the ferromagnetic alloy – ferroelectric ceramics nanocomposite $(FeCoZr)_x(PbZrTiO_3)_{(100-x)}$ of similar metallic phase contents have been produced using ion-beam sputtering in the atmosphere of argon and oxygen. The samples have been produced in order to examine the influence of sputtering atmosphere parameters on electrical properties of the tested materials.

In a nanocomposite of a reduced oxygen content, a conductivity increase by about three orders occurs along with the increasing frequency, which is associated with the occurrence of hopping recharging. Over the whole area of low measuring frequencies, negative values of the phase shift and a capacitive type of conductivity occur. For the frequency of about 10^6 Hz, the phase shift reaches zero, which corresponds to the voltage resonance phenomenon. For higher frequencies, positive phase shift values and inductive conductivity occur. For a sample of a higher oxygen content, phenomena of voltage resonance (low frequency values) and current resonance (high frequency values) can be observed. When the oxygen content increases, frequency dependences of the phase difference get shifted into the low frequency area. This is associated with the surface oxidation or a complete oxidation of the metallic-phase nanograins, which increases the potential barrier as well as with an increase of the relaxation time activation energy. For the sample of a higher oxygen content, an increase of the conductivity activation energy has been observed in the low temperature area.

1. Introduction

Currently used methods for producing nanomaterials and various multilayer coatings [1–3] meet keen interest of researchers all over the world [4–11]. Such an attention follows from a great variety of nanomaterials that can be manufactured using that type of techniques. These materials are very appealing mainly owing to their unique mechanical [12,13], electrical [14–16], magnetic [17–22] and optical [23–26] properties, which makes them advantageously applicable in the areas of medicine, technology and industry. Enhancement of the manufacturing methods as well as providing higher quality of the produced nanostructures and multi-layer films make the most topical issues at the present time [27,28]. Basic methods for producing nanostructured materials can be analyzed into two types: the "top down" ones that apply breaking up of solid materials to obtain nano-dimensions (lithography, ball grinding, etc.) [29,30] and the "bottom up" one that consist in the "atom by atom" formation of nanostructures.

Among the "bottom up" techniques such ones as: ion [31,32] and magnetron sputtering [33,34], ion implantation [35,36], plasma techniques [37,38] and chemical methods [39] should be distinguished for their advantageous application to the development of nano-sized materials. These methods consist in transiting the material from its solid state (referred to as a target) into the gaseous phase followed by its deposition onto the substrate. The ion implantation method that applies high ion doses deserves a particular attention. In this case, when the solubility threshold for the impurity atoms in the matrix material gets exceeded, the ions driven into the solid body begin to form the second-phase clusters that can be nano-sized [40]. The "bottom-up" methods can be used to produce nanomaterials of both crystalline and amorphous structures and varied chemical composition. It should be noted that the ion sputtering technique applied to produce nano-sized materials essentially affects their physical-chemical properties. It is very important to adequately select the precursors, the

* Corresponding author.
E-mail address: t.koltunowicz@pollub.pl (T.N. Koltunowicz).

http://dx.doi.org/10.1016/j.ceramint.2016.11.052
Received 17 October 2016; Received in revised form 3 November 2016; Accepted 3 November 2016
Available online 11 November 2016

reaction medium and the synthesis parameters such as temperature, pressure or pH.

The objective of the presented paper have been to compare electrical properties of the nanocomposite $(FeCoZr)_x(PbZrTiO_3)_{(100-x)}$, produced by ion sputtering with a combined beam of argon and oxygen ions of varied ratio of the oxygen ion content to the content of argon ions.

2. Experimental

In order to investigate the impact of the sputtering atmosphere parameters on electrical properties of metal-dielectric nano-films, two sample sets of the $(FeCoZr)_x(PbZrTiO_3)_{(100-x)}$ nanocomposite of similar metallic phase contents have been produced. Those nanostructures have been prepared using ion-beam sputtering applied to a target composed of a plate of the metallic alloy ($Fe_{0.45}Co_{0.45}Zr_{0.10}$) and strips of the dielectric – ferroelectric ceramics $PbZrTiO_3$ attached to the plate. The sputtering has been performed in the atmosphere of Ar and O_2 with the application of different partial pressures to those two sample sets. Partial pressures applied to the first testing series (sample x_1) have been of $P(Ar)_1=6.6\times10^{-2}$ Pa and $P(O_2)_1=2\times10^{-3}$ Pa (material of a lower oxygen content in the sputtering beam), while for the other testing series (sample x_2) partial pressures of $P(Ar)_2=7.4\times10^{-2}$ Pa and $P(O_2)_2=3\times10^{-3}$ Pa (material of a higher oxygen content in the sputtering beam) have been used. The films have been deposited on water-cooled glass-ceramic substrates. Technological details of the film preparation process can be found in [41,42]. Preliminary testing and a comparative analysis of nanocomposites characterized by a similar phase composition, such as $(FeCoZr)_x(CaF_2)_{(100-x)}$, and $(FeCoZr)_x(Al_2O_3)_{(100-x)}$ [31,43], have shown that it is impossible to deposit a stable nano-film of the ferromagnetic alloy – ferroelectric ceramics $(FeCoZr)_x(PbZrTiO_3)_{(100-x)}$ in the atmosphere of pure argon. It has been found that in the case of the tested films the only way to stabilize their nanogranular structure is to add oxygen to the synthesis atmosphere. Energy Dispersive X-ray analysis (EDX) has been applied to determine elemental composition of the nanocomposite $(FeCoZr)_x(PbZrTiO_3)_{(100-x)}$. The analysis of light elements (O_2) has been performed using the Rutherford backscattering spectroscopy (RBS) technique. Interdependence of the metallic (x_1 and x_2) and dielectric ($(1-x_1)$ and $(1-x_2)$) phases has been experimentally determined as a ratio of total concentrations of component metals of the tested ferroelectric alloy (Fe, Co, Zr) to the components of the dielectric matrix (Pb, Zr, Ti, O). Detailed discussion of investigations into the structure and chemical composition of the $(FeCoZr)_x(PZT)_{(100-x)}$ nanocomposites can be found in [44].

Measurements of electrical parameters (capacitance C_p, conductivity σ, the phase difference θ) have been performed in an equivalent parallel system using alternating current of the frequency range 50 Hz – 5×10^6 Hz. The measuring temperature effect on electrical parameters of the nano films has been tested for the temperature range from 15 K to 375 K. The experimental setup that has been applied to measure AC electrical properties of nanocomposites is presented in [45,46]. The measurements have been realized for samples sized: 10 mm in length, 3 mm in width and 1 μm in thickness. Silver contacts (2×3 mm^2) have been applied at both ends of the samples.

3. Analysis of measurement results

Comparative testing of nanocomposites $(FeCoZr)_x(PbZrTiO_3)_{(100-x)}$ has been performed using two samples of similar metallic phase contents: $x_1=51.7$ at% in the first series of a lower oxygen content in the sputtering ion-beam and $x_2=52.0$ at% in the second series of a higher oxygen content. In both cases, the materials are below the percolation threshold and exhibit conductivity of the dielectric type i.e. conductivity of the films increases along with the growing temperature.

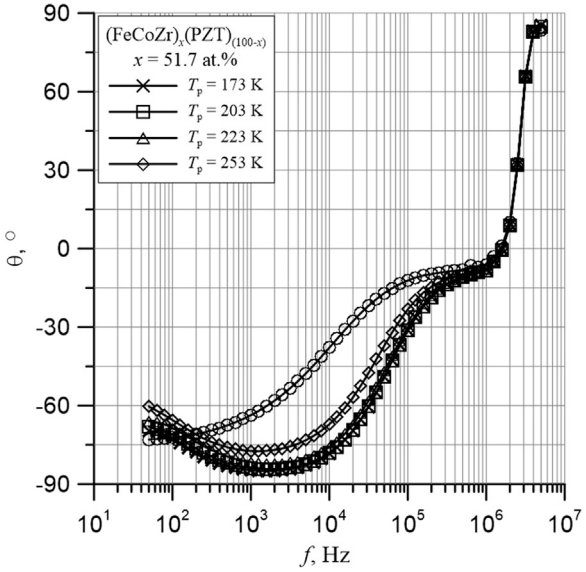

Fig. 1. Phase difference θ vs. frequency for the $(FeCoZr)_{51.7}(PbZrTiO_3)_{48.3}$ nanocomposite sample of a lower oxygen content.

Figs. 1 and 2 show phase difference θ vs. frequency characteristics obtained for samples of the nanocomposite $(FeCoZr)_x(PbZrTiO_3)_{(100-x)}$ of the metallic phase content $x_1=51.7$ at% (lower oxygen content) and $x_2=52.0$ at% (higher oxygen content) and four selected measuring temperatures: 173 K, 203 K, 223 K and 253 K. Similar measuring temperatures have been applied in the cases shown in Figs. 4–7. As can be seen in Fig. 1, in the range of measuring frequencies up to 10^6 Hz the phase difference assumes negative values. Temperature dependence of the angle θ also occurs. It means that within the mentioned frequency area the nanocomposite conductivity can be defined as capacitive, which is characteristic for nanocomposites of different contents of the metallic phase FeCoZr produced in the argon atmosphere of a low oxygen content $P(O_2)_1=2\times10^{-3}$ Pa [47]. For the frequencies exceeding 10^6 Hz positive phase difference values occur, which corresponds to the inductive type of conductivity.

As can be seen in Fig. 2, it is characteristic for the material produced with a beam of a higher oxygen content that in the frequency area of 50–500 Hz a dependence of capacitive conductivity on the measuring temperature occurs. On the other hand, in the area of higher

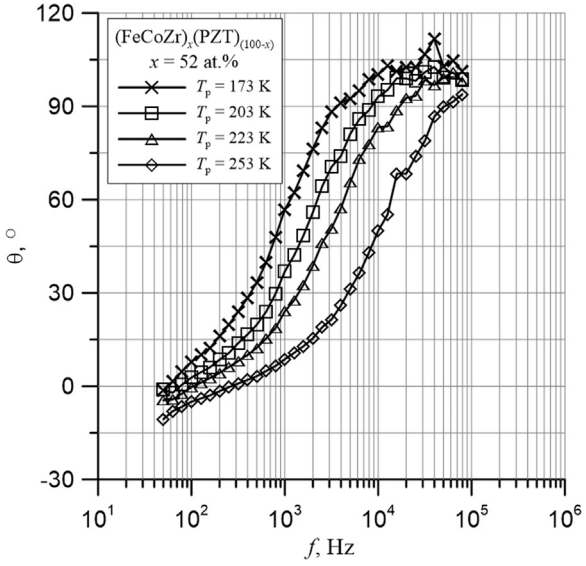

Fig. 2. Phase difference θ vs. frequency for the $(FeCoZr)_{52}(PbZrTiO_3)_{48}$ nanocomposite sample of a higher oxygen content.

frequencies positive phase shift values can be observed, which indicates the inductive component of electrical conduction. Conductivity of the inductive type is realized by a hopping exchange of electric between nanoparticles of the metallic phase FeCoZr (potential wells) randomly distributed in the matrix of ferroelectric ceramics $PbZrTiO_3$. A model of that conduction mechanism is discussed in [48,49]. According to that model, an electron hop from the first FeCoZr nanoparticle to the other one is realized within the time span of the 10^{-13} s order. A return hop of that electron back to the original nanoparticle occurs after a lapse of the time τ (dipole lifetime), which takes much longer that is from 10^{-3} to 10^{-7} s, depending on the metallic phase content and the temperature. When AC voltage of the frequency of $f > 1/\tau$ is applied, phase lag of the return hop can exceed $3/2\pi$, which results in the occurrence of positive phase shift values. In case of the nanocomposite $(FeCoZr)_{51.7}(PbZrTiO_3)_{48.3}$ (lower oxygen content in the sputtering beam) the zero-crossing of the phase difference is practically independent of the measuring temperature (Fig. 1). In contrast, Fig. 2 shows temperature dependence of that point obtained for the sample x_2 that is characterized by a high oxygen content in the sputtering beam. That zero crossing corresponds to the resonance frequency f_R and the relaxation time $\tau \sim 1/f_R$. The relaxation time is an exponential function of the activation energy [50,51]:

$$\tau_R(T) = \tau_0 \cdot \exp\left(\frac{\Delta E_\tau}{kT}\right) \quad (1)$$

Activation energy of the relaxation time has been determined using Arrhenius plots.Fig. 3 presents Arrhenius plots for the relaxation time values determined based on Figs. 1 and 2 for the points, where the phase shift crosses zero. For samples of low oxygen content, the relaxation time value is practically independent of the measuring temperature. This is easy to explain, considering that the electron tunneling takes place between nanoparticles of the metallic phase. The tunneling is realized from the first level below the Fermi level to the first level above the Fermi level. As can be seen in Fig. 3, distances between energy levels in the nanoparticles range below 1 meV depending on the number of atoms in them. Hence the negligibly low activation energy of the relaxation time.

In the nanocomposite $(FeCoZr)_x(PbZrTiO_3)_{(100-x)}$ of a higher oxygen content, in the area of low temperatures, the relaxation time activation energy is 46 meV (Fig. 3), and in the temperature area of above 225 K the relaxation time activation energy increases up to 352 meV. In our opinion, those high activation energy values in the

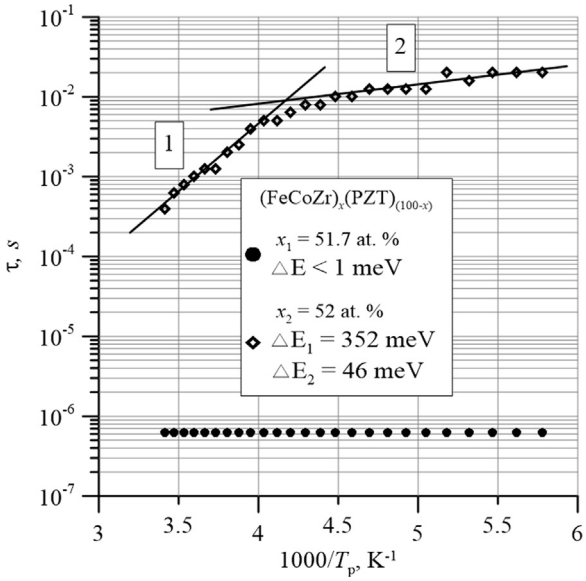

Fig. 3. Arrhenius plots of relaxation times for the $(FeCoZr)_x(PbZrTiO_3)_{(100-x)}$ nanocomposite samples of lower and higher oxygen contents.

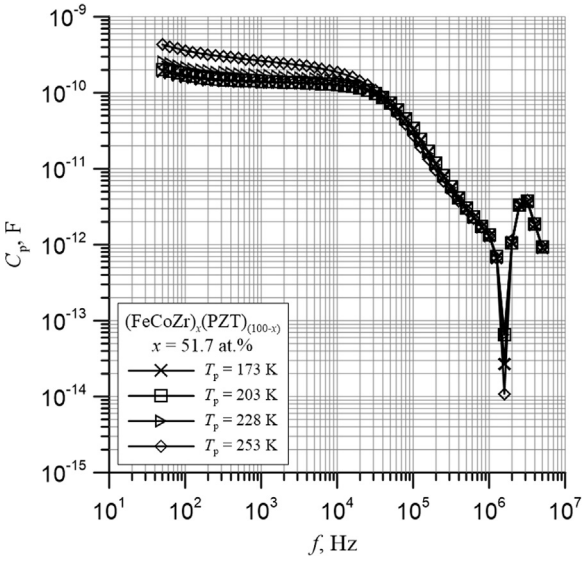

Fig. 4. Capacity C_p vs. frequency for the $(FeCoZr)_{51.7}(PbZrTiO_3)_{48.3}$ nanocomposite sample of a lower oxygen content.

nanocomposite of a higher oxygen content in the synthesis atmosphere are related to the fact that a part of the nanograins gets oxidized on their surface, which results in the formation of a potential barrier that impedes the electron tunneling and in the activation energy increase in the low temperature area up to the value of ΔE_2=46 meV. Probably, a considerable part of the metallic-phase nanoparticles gets completely oxidized. In their case the electron tunneling is realized between energy levels on the surface of those metal-oxide nanoparticles, which further increases the relaxation time activation energy in the area of higher temperatures up to the value of ΔE_1=352 meV, which can be seen in Fig. 3.

Figs. 4 and 5 show selected frequency dependences of capacity for nanocomposite samples produced with the application of lower and higher oxygen contents in the synthesis atmosphere. As can be seen in Fig. 4, for the frequency range of 50–10^4 Hz, capacity of the sample x_1 of a lower oxygen content is almost independent of the frequency and assumes the value of approx. 2×10^{-9} F. At frequency values exceeding 10^4 Hz, a decrease of the capacity can be observed. At the frequency of 10^6 Hz a distinct minimum can be seen. It is related to the occurrence of the voltage resonance phenomenon, which is additionally shown by the zero crossing by the phase difference (Fig. 1).

In Fig. 5, for a sample x_2 of a higher oxygen content, sharp minima can be seen in the $C_p(f)$ characteristics in the low frequency area. A comparative analysis of the capacity (Fig. 5) and the phase shift (Fig. 2) characteristics shows that the minimum on the capacity dependence exactly coincides with the frequency f_R for which θ=0°, which is characteristic for the voltage resonance occurrence in conventional serial RLC circuits. In the frequency area above the sharp minimum, a smooth capacity decrease by an order of magnitude can be observed (Fig. 5).

The occurrence of capacity minima at the resonance frequency (Figs. 4 and 5) is related to the measurement procedure using an impedance meter. In the tested material, a simultaneous occurrence of the inductive and a capacitive components of opposite phases (−90° and +90°) can be observed. At the frequency f_R, their voltage drop values are equal. As the capacitive and inductive components cannot be measured simultaneously, the capacity values have been calculated based on the reactive component measurements *of* voltage of the reactive component can be calculated using the below formula [52]:

$$U = i_0\left(\omega L_S - \frac{1}{\omega C_S}\right) \quad (2)$$

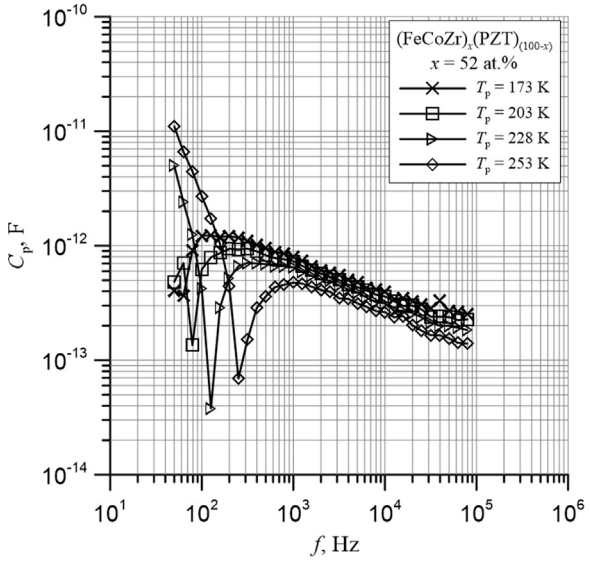

Fig. 5. Capacity C_P vs. frequency for the $(FeCoZr)_{52}(PbZrTiO_3)_{48}$ nanocomposite sample of a higher oxygen content.

where: i_0 – exciting current amplitude; C_S – capacity; L_S – circuit inductance; ω – pulsatance

which in the voltage resonance case can be written as follows:

$$U_R = i\left(\omega_R L_S - \frac{1}{\omega_R C_S}\right) = 0 \tag{3}$$

where $\omega_R=2\pi f_R$.

It follows from the Formula (3) that at the resonance frequency the measured capacitance assumes a very low value (theoretically – zero, practically – about 5×10^{-14} F).

Figs. 6 and 7 show frequency dependences of the nanocomposite conductivity for selected testing temperatures. Fig. 6 shows that in the case of the sample x_1 (lower oxygen content) the conductivity vs. frequency dependence is very strong (of approximately three orders of magnitude) and grows along with the increasing measuring frequency. It clearly indicates the hopping mechanism (tunneling) of the charge exchange between metallic phase [48,49,53]. As can be seen in Fig. 7, the conductivity vs. frequency dependence is much weaker in the case of the sample x_2 (higher oxygen content). Within the frequency range of

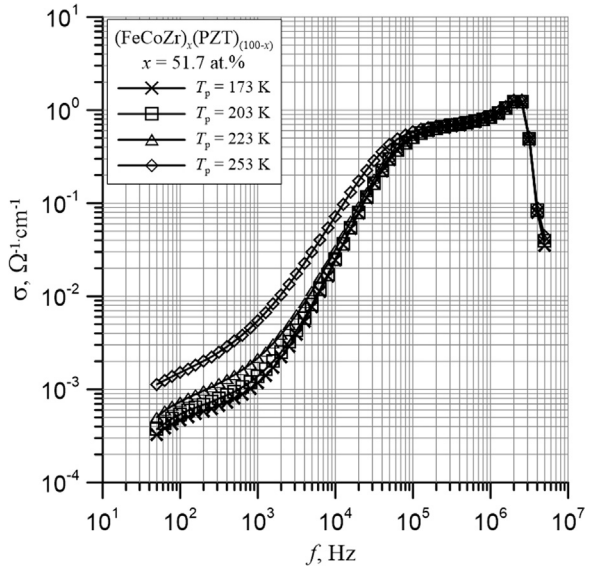

Fig. 6. Conductivity σ vs. frequency for the $(FeCoZr)_{51.7}(PbZrTiO_3)_{48.3}$ nanocomposite sample of a lower oxygen content.

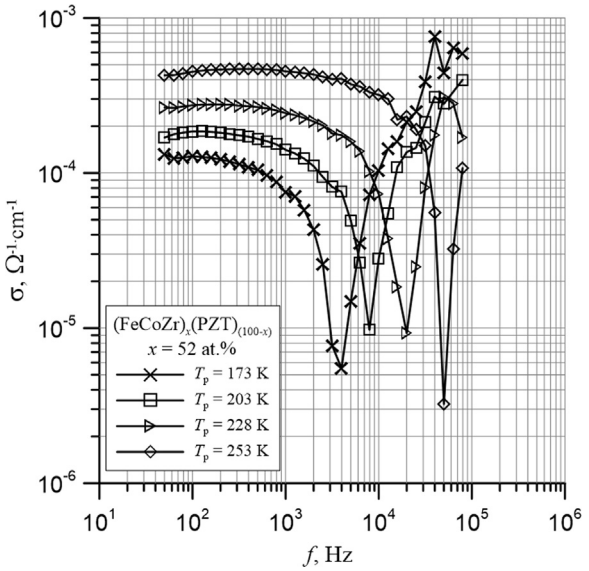

Fig. 7. Conductivity σ vs. frequency for the $(FeCoZr)_{52}(PbZrTiO_3)_{48}$ nanocomposite sample of a higher oxygen content.

10^3–10^5 Hz, distinct minima can be seen in the σ(*f*) characteristics. Frequency values at which the θ(*f*)=90° occurs (Fig. 2) coincide with the minima in the σ(*f*) characteristics (Fig. 7), which indicates that in the nanocomposite of a higher oxygen content current resonance, occurs in circuits with conventional RLC elements connected in parallel. Analyses have shown that in order to determine electrical phenomena that occur in the nanocomposite $(FeCoZr)_{52}(PbZrTiO_3)_{48}$, produced by sputtering with a beam of argon and oxygen, a combined series-parallel circuit connection system of conventional RLC elements should be used. An equivalent circuit for such a nanocomposite is shown in Fig. 8. The series connections of the system are responsible for the voltage resonance occurrence, while the parallel circuits– for the current resonance phenomena.

4. Summary

The ion-beam sputtering technique using varied parameters of the synthesis atmosphere has been applied to produce samples of the nanocomposite $(FeCoZr)_x(PbZrTiO_3)_{(100-x)}$ of similar metallic phase contents of x_1=51.7 at% and x_2=52 at%. In order to determine the impact of the sputtering atmosphere parameters on electrical properties of the $(FeCoZr)_x(PbZrTiO_3)_{(100-x)}$ nanocomposite, a comparative analysis of the frequency and temperature dependences of the phase difference, capacity and conductivity of the tested materials has been performed.

In the case of a nanocomposite produced with a beam of a lower oxygen content (sample x_1), its conductivity has increased by ca 3 orders along with the increasing frequency, which indicates the occurrence of the hopping charge exchange in the material. An electron hop from one neutral nanoparticle to another brings about a hopping conductivity and the formation of electric dipoles, which results in an increase of the nanocomposite permittivity in the low frequency area. Negative phase shift values in the frequency area up to 10^6 Hz indicate conductivity of the capacitive type. At the frequency of about 10^6 Hz the phase shift reaches the zero value, which is characteristic for the

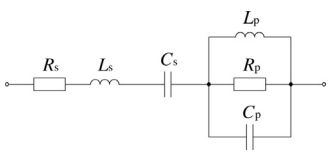

Fig. 8. Equivalent circuit for the $(FeCoZr)_{52}(PbZrTiO_3)_{48}$ nanocomposite sample.

occurrence of the voltage resonance phenomenon in the material. Further frequency increase causes the phase shift transition into the area of positive values, which shows the occurrence of the inductive conductivity component in the material.

In a sample produced in the atmosphere of a higher oxygen content (sample x_2), the phenomena of voltage (low frequency area) and current (high frequency area) resonance occur. The current resonance phenomenon is represented by a sharp minimum in the conductivity vs. frequency characteristic and the phase shift value of θ=+90° Additionally, an increased oxygen content in the sputtering beam brings about a shift of the phase difference vs. frequency characteristic of into the low frequency area. It is related to the oxidation processes on the surface of the metallic nanograins or their complete oxidation. In effect, an increase of the potential barrier occurs followed by an increase of the relaxation time activation energy, which leads to the shift of the phase difference vs. frequency characteristics into the low frequency area as compared to the sample of a lower oxygen content.

Acknowledgements

The presented research project has been financially supported within the framework of the statutory activity grants of the Lublin University of Technology, Faculty of Electrical Engineering and Computer Science Grant No 8620/E-361/S/2016 (S-28/E/2016) entitled "*Investigations into electrical, magnetic, thermal and mechanical properties of modern electrotechnical and electronic materials, including nanomaterials, and electrical devices and their components, in order to determine their applicability in electrical engineering and to enhance the energy management efficiency*" and the statutory activity of young researchers grant No 8620/E-361/M/2016 (S-280/E/2016), entitled "*Investigations into electrical, optical, mechanical and structural properties of selected nanocomposites*".

References

[1] A.D. Pogrebnjak, O.M. Ivasishin, V.M. Beresnev, Arc-evaporated nanoscale multilayer nitride-based coatings for protection against wear, corrosion, and oxidation, Usp. Fiz. Met. 17 (1) (2016) 1–28.
[2] A.D. Pogrebnjak, I.V. Yakushchenko, O.V. Bondar, V.M. Beresnev, K. Oyoshi, O.M. Ivasishin, H. Amekura, Y. Takeda, M. Opielak, C. Kozak, Irradiation resistance, microstructure and mechanical properties of nanostructured (TiZrHfVNbTa)N coatings, J. Alloy. Compd. 679 (2016) 155–163.
[3] S.N. Bratushka, M. Opielak, S. Liscak, Structure and properties of Co-Cr coatings after a pulsed jet treatment, Prz. Elektrotech. 88 (10A) (2012) 314–318.
[4] H.C. Barshilia, B. Deepthi, K.S. Rajam, K.P. Bhatti, S. Chaudhary, Growth and haracterization of TiAlN/CrAlN superlattices prepared by reactive direct current magnetron sputtering, J. Vac. Sci. Technol. A Vac. Surf. Film 27 (2009) 29–36.
[5] J. Musil, P. Baroch, J. Vlček, K.H. Nam, J.G. Han, Reactive magnetron sputtering of thin films: present status and trends, Thin Solid Films 475 (2005) 208–218.
[6] L. Signorini, L. Pasquini, L. Savini, R. Carboni, F. Boscherini, E. Bonetti, A. Giglia, M. Pedio, N. Mahne, S. Nannarone, Size-dependent oxidation in iron/iron oxide core-shell nanoparticles, Phys. Rev. B 68 (195423) (2003).
[7] L. Del Bianco, D. Fiorani, A.M. Testa, E. Bonetti, L. Savini, S. Signoretti, Magnetothermal behavior of a nanoscale Fe/Fe oxide granular system, Phys. Rev. B 66 (174418) (2002).
[8] J.A. Davis, D.K. Brown, W. Henderson, Fractal electrode formation in metal-insulator composites near the percolation threshold, IEEE Trans. Nanotechnol. 12 (5) (2013) 725–733.
[9] A.D. Pogrebnjak, Structure and properties of nanostructured (Ti-Hf-Zr-V-Nb)N coatings, J. Nanomater. (2013) 780125.
[10] A.D. Pogrebnjak, V.M. Beresnev, A.A. Demianenko, V.S. Baidak, F.F. Komarov, M.V. Kaverin, N.A. Makhmudov, D.A. Kolesnikov, Adhesive strenght, superhadness, and the phase and elemental composition of nannostructured coating based Ti-Hf-Si-N, Phys. Solid State 54 (9) (2012) 1882–1890.
[11] A.D. Pogrebnjak, A.A. Bagdasaryan, I.V. Yakushchenko, V.M. Beresnev, The structure and properties of high-entropy alloys and nitride coatings based of them, Russ. Chem. Rev. 83 (11) (2014) 1027–1061.
[12] N.I. Poliak, V.M. Anishchik, N.G. Valko, C. Karwat, C. Kozak, M. Opielak, Mechanical properties of Zn-Ni-SiO_2 coating deposited under x-ray irradiation, Acta Phys. Pol. A 125 (6) (2014) 1415–1417.
[13] A.H. Ramezani, M.R. Hantehzadeh, M. Ghoranneviss, E. Darabi, Mechanical and electrochemical properties of tantalum implanted by nitrogen ions, High. Temp. Mater. Process. 18 (1–2) (2014) 143–153.
[14] T.N. Koltunowicz, Dielectric properties of $(CoFeZr)_x(PZT)_{(100-x)}$ nanocomposites produced with a beam of argon and oxygen ions, Acta Phys. Pol. A 125 (6) (2014) 1412–1414.
[15] Y. Imry, Introduction to Mesoscopic Physics, 2nd ed., Oxford University Press, Oxford, New York, 2002, p. 236.
[16] S.K. Moosvi, K. Majid, T. Ara, Synthesis and characterization of PPY/K[Fe(CN)(3)(OH)(en)] nanocomposite: study of photocatalytic, sorption, electrical, and thermal properties, J. Appl. Polym. Sci. 133 (23) (2016). http://dx.doi.org/10.1002/app.43487.
[17] D.L. Peng, T. Hihara, K. Sumiyama, H. Morikawa, Structural and magnetic characteristics of monodispersed Fe and oxide-coated Fe cluster assemblies, J. Appl. Phys. 92 (2002) 3075–3083.
[18] Q.K. Ong, A. Wei, X.-M. Lin, Exchange bias in Fe/Fe_3O_4 core-shell magnetic nanoparticles mediated by frozen interfacial spins, Phys. Rev. B 80 (134418) (2009).
[19] Z. Turgut, N.T. Nuhfer, H.R. Piehler, M.E. McHenry, Magnetic properties and microstructural observations of oxide coated FeCo nanocrystals before and after compaction, J. Appl. Phys. 85 (1999) 4406–4408.
[20] P. Zhukowski, J. Sidorenko, T.N. Kołtunowicz, J.A. Fedotova, A.V. Larkin, Magnetic properties of nanocomposites $(CoFeZr)_x(Al_2O_3)_{1-x}$, Prz. Elektrotech. 86 (7) (2010) 296–298.
[21] J.V. Kasiuk, J.A. Fedotova, T.N. Koltunowicz, P. Zukowski, A.M. Saad, J. Przewoznik, Cz Kapusta, J. Zukrowski, I.A. Svito, Correlation between local Fe states and magnetoresistivity in granular films containing FeCoZr nanoparticles embedded into oxygen-free dielectric matrix, J. Alloy. Compd. 586 (Suppl. 1) (2014) S432–S435.
[22] H. Sharma, S. Jain, P.M. Raj, K.P. Murali, R. Tummala, Magnetic and dielectric property studies in Fe- and NiFe-based polymer nanocomposites, J. Electron. Mater. 44 (10) (2015) 3819–3826.
[23] A. Moradi, Plasmonic waves of random metal-dielectric nanocomposite films, Photonics Nanostruct. Fundam. Appl. 15 (2015) 41–45.
[24] C. Gavade, N.L. Singh, P.K. Khanna, Optical and dielectric properties of ion beam irradiated Ag/polymethyl methacrylat nanocomposites, J. Nanosci. Nanotechnol. 14 (8) (2014) 5911–5916.
[25] N. Zhang, K. Liu, H.M. Song, Z.J. Liu, D.X. Ji, X. Zeng, S.H. Jiang, Q.Q. Gan, Refractive index engineering of metal-dielectric nanocomposite thin films for optical super absorber, Appl. Phys. Lett. 104 (20) (2014), 203112.
[26] A. Moradi, Optical properties of random metal-dielectric nanocomposite films: nanoparticle size effects, Phys. Scr. A 90 (9) (2015), 095803.
[27] W.F. Piedrahita, L.E. Coy, C. Amaya, I. Llarena, J.C. Caicedo, L. Yate, Influence of the negative R.F. bias voltage on the structural, mechanical and electrical properties of Hf-C-N coatings, Surf. Coat. Technol. 286 (2016) 251–255.
[28] S. Veprek, M.G.J. Veprek-Heijman, P. Karvankova, J. Prochazka, Different approaches to superhard coatings and nanocomposites, Thin Solid Films 476 (2005) 1–29.
[29] L.N. Mishnina, L.A. Selyunina, T.M. Botvina, Synthesis and characteristics of $CaAl_2O_4$:Eu^{3+} phosphor prepared by zol-gel method, Key Eng. Mater. 670 (2016) 95–100.
[30] D.H. Kuang, P. Tang, S.H. Yang, Y.L. Zhang, Effect of annealing temperatures on the structure and leakage mechanisms of BiFeO3 thin films prepared by the sol–gel method, J. Sol-Gel Sci. Technol. 73 (2) (2015) 410–416.
[31] T.N. Koltunowicz, P. Zukowski, V. Bondariev, A.K. Fedotov, I. Svito, J. Fedotova, A. Saad, Voltage and current resonance in nanocomposite $(FeCoZr)_x(CaF_2)_{(100-x)}$ produced by ion-beam sputtering in pure argon atmosphere, Acta Phys. Pol. A 128 (5) (2015) 897–900.
[32] L. Zhang, S. Tong, H. Liu, Y. Li, Z. Wang, Effects of sputtering and assisting ions on the orientation of titanium nitride films fabricated by ion beam assisted sputtering deposition from metal target, Mater. Lett. 171 (2016) 304–307.
[33] K.X. Sun, S.Y. Zhang, K. Wasa, X.J. Shui, Characterization of La-doped $xBiInO_3(1-x)PbTiO_3$ piezoelectric films deposited by the radio-frequency magnetron sputtering method, Chin. Phys. Lett. 33 (064301) (2016) 6.
[34] L. Guo, M. Zhao, D. Zhuang, Q. Gong, H. Tan, M. Cao, L. Ouyang, A study on phase transformation of SnO_x thin films prepared by reactive magnetron sputtering, Mater. Sci. Semicond. Process. 46 (2016) 35–38.
[35] H. Shang, J. Fu, C. Xie, Z. Li, D. Chen, Improving stress stability in low-pressure chemical vapor deposited silicon dioxide films by ion implantation, Thin Solid Films 598 (2016) 103–108.
[36] M.A. Sortica, B. Canut, M. Hatori, J.F. Dias, N. Chauvin, O. Matry, Optical and structural properties of InAs nanoclusters in crystalline Si obtained through sequential ion implantation and RTA, Phys. Status Solidi A 212 (12) (2015) 2686–2691.
[37] A.D. Pogrebnjak, M.M. Danilionokc, V.V. Uglov, N.K. Erdybaeva, G.V. Kirik, S.N. Dub, V.S. Rusakov, A.P. Shypylenko, P.V. Zukovski, Y.Zh Tuleushev, Nanocomposite protective coatings based on Ti–N–Cr/Ni–Cr–B–Si–Fe, their structure and properties, Vacuum 83 (Suppl. 1) (2009) S235–S239.
[38] Y. Miao, X. Wang, P. Firbas, K. Wang, Z. Yang, B. Liang, Y. Cheng, D. Jia, Ultra-fine zirconium diboride powders prepared by a combined sol–gel and spark plasma sintering technique, J. Sol-Gel Sci. Technol. 77 (2016) 636–641.
[39] Gomaa A.M. Ali, Mashitah M. Yusoff, Yun Hau Ng, Hong Ngee Lim, Kwok Feng Chong, Potentiostatic and galvanostatic electrodeposition of manganese oxide for supercapacitor application: a comparison study, Curr. Appl. Phys. 15 (2015) 1143–1147.
[40] F.F. Komarov, L.A. Vlasukova, O.V. Milchanin, M. Makhavikou, I. Parkhomenko, E. Wendler, W. Wesch, G. Ismailova, M. Opielak, Thin films of SiO_2 ion-implanted with Sn: evaluation of structure and composition, in: A. Grigonis (Ed.), Proceedings of the 5th International Conference Radiation Interaction with Materials: Fundamentals and Applications, 2014, pp. 385–388.
[41] E. Yu, A.T. Kalinin, A.V. Ponomarenko, O.V. Sitnikov, Stogney, Granular metal-

insulator nanocomposites with amorphous structure, Phys. Chem. Mater. Treat. 5 (2001) 14–20.
[42] I.V. Zolotukhin, Yu.E. Kalinin, A.T. Ponomarenko, V.G. Shevchenko, A.V. Sitnikov, O.V. Stognei, O. Figovsky, Metal-dielectric nanocomposites with amorphous structure, J. Nanostruct. Polym. Nanocompos. 2 (2006) 23–34.
[43] I. Svito, J.A. Fedotova, M. Milosavljević, P. Zhukowski, T.N. Koltunowicz, A. Saad, K. Kierczynski, A.K. Fedotov, Influence of sputtering atmosphere on hopping conductance in granular nanocomposite $(FeCoZr)_x(Al_2O_3)_{1-x}$ films, J. Alloy. Compd. 615 (Suppl. 1) (2014) S344–S347.
[44] J.V. Kasiuk, J.A. Fedotova, M. Marszalek, A. Karczmarska, M. Mitura-Nowak, Yu.E. Kalinin, A.V. Sitnikov, Effect of oxygen pressure on phase composition and magnetic structure of FeCoZr–$Pb(ZrTi)O_3$ nanocomposites, Phys. Solid State 54 (1) (2012) 178–184.
[45] T.N. Koltunowicz, Measurement station for frequency dielectric spectroscopy of nanocomposites and semiconductors, J. Appl. Spectrosc. 82 (4) (2015) 653–658.
[46] F.F. Komarov, P. Zhukowski, R.M. Krivosheev, E. Munoz, T.N. Koltunowicz, V.N. Rodionova, A.K. Togambaeva, Effects of surfactant and fabrication procedure on the electrical conductivity and electromagnetic shielding of single-walled carbon nanotube films, Phys. Status Solidi A – Appl. Mater. Sci. 212 (2) (2015) 425–432.
[47] T.N. Koltunowicz, P. Zukowski, O. Boiko, K. Czarnacka, V. Bondariev, A. Saad, A.V. Larkin, A.K. Fedotov, Capacitive properties of nanocomposite $(FeCoZr)_x(PZT)_{(100-x)}$ produced by sputtering with the use of argon and oxygen ions beam, J. Mater. Sci. Mater. Electron. 27 (2016) 1171–1176.
[48] T.N. Koltunowicz, P. Zukowski, O. Boiko, A. Saad, J.A. Fedotova, A.K. Fedotov, A.V. Larkin, J. Kasiuk, AC hopping conductance in nanocomposite films with ferromagnetic alloy nanoparticles in a $PbZrTiO_3$ matrix, J. Electron. Mater. 44 (7) (2015) 2260–2268.
[49] T.N. Kołtunowicz, P. Żukowski, O. Boiko, V. Bondariev, K. Czarnacka, J.A. Fedotova, A.K. Fedotov, I.A. Svito, Impedance model of metal-dielectric nanocomposites produced by ion-beam sputtering in vacuum and its experimental verification for thin films of $(FeCoZr)_x(PZT)_{(100-x)}$, Vacuum 120 (Part B) (2015) 37–43.
[50] G.C. Psarras, E. Manolakaki, G.M. Tsangaris, Dielectric dispersion and AC conductivity in Iron particles loaded-polymer composites, Composites Part A 34 (12) (2003) 1187–1198.
[51] M.A. Kudryashov, A.I. Mashin, A.A. Logunov, G. Chidichimo, G. De Filpo, Frequency dependence of the electrical conductivity in Ag/PAN nanocomposites, Tech. Phys. 57 (7) (2012) 965–970.
[52] D. Haliday, R. Resnik, Physics, Part II, Willey and Sons, Inc., New York, 1962.
[53] N.F. Mott, E.A. Davis, Electron Processes in Non-crystalline Materials, Clarendon, Oxford, 1979.